ARMA 10-520

Stimulated Fractured Reservoir DFN Models Calibrated with Microseismic Source Mechanisms

Williams-Stroud, S. C. and Eisner, L.
MicroSeismic, Inc., Houston, TX, USA

This paper was prepared for presentation at the 44th US Rock Mechanics Symposium and 5th U.S.-Canada Rock Mechanics Symposium, held in Salt Lake City, UT June 27–30, 2010.

ABSTRACT: Methods for constraining discrete fracture network (DFN) models have historically relied on two very different scales for data: large-scale sources from which attributes can be coarsely defined for volume elements of 1000s of cubic meters such as seismic data, or small-scale sources where attributes of individual fractures are measured on a meter scale such as wellbores. Populating reservoir models with wellbore data requires upscaling the measured parameters, and the use of the large scale data types is accompanied by assumptions that can have significant uncertainties. A source of data that fills the gap intermediate to the large and small scale fracture parameters is microseismic data. During reservoir stimulation or production, acquisition of microseismic data with a surface array of geophones laid out in multiple azimuths and offsets (e.g., a star-like pattern above the well, or shallowly buried geophones in a grid like pattern), provides a broad sampling of the focal sphere that can be used to invert microseismic events for the source mechanism. This paper presents examples of DFN models constrained with source mechanisms and the implications for reservoir modeling of these more-highly constrained fracture network models.

1. INTRODUCTION

Induced seismicity can be caused by various reservoir activities such as hydraulic fracturing, water injection or fluid extraction. Tight gas and oil shales have increase in importance as reservoir rocks, and hydraulic fracturing stimulation is required for their economic production. Monitoring the induced seismicity from the stimulations has been increasingly used to optimize hydraulic fracturing design and optimize oil and gas field development and production. This optimization is usually derived from the geometrical distribution of the located microseismic events. However, seismic waveforms recorded by various monitoring systems carry additional information on the mechanism of failure for each of these events. The event source mechanisms can be used to directly quantify and qualify stress changes instead of inferring these changes from the spatial distribution of the located microseismic events. Locations are derived mainly from observed arrival times while source mechanisms are inverted from relative amplitudes of either P or S waves (or both). Arrival times are less sensitive to small perturbations resulting from medium heterogeneity in a reservoir so locations are possible to achieve with a small aperture monitoring array, such as those placed down hole in a well near the well being stimulated.. Given that most of the early monitoring studies were carried out only with this type of very limited aperture array, source mechanism inversions from the uncertainty due to limited observation points produced unreliable results. The source mechanism inversion became more stable with larger numbers of monitoring receivers, such as can be deployed with multiple monitoring boreholes, or as a network of receivers distributed on the surface, or in the shallow subsurface. With larger numbers of monitoring receivers over a larger area there are geophones at multiple offsets and azimuths. The broader aerial coverage of such a receiver network can compensate for lower signal-to-noise ratio and provide more precise and accurate locations and source mechanisms.

Microseismic mapping during reservoir stimulation is used to define the extent of fracture activity related to stimulation treatment. Spatial trends of events can be interpreted to define a fracture plane, but source mechanism inversion on microseismic events provides more specific information about the size, orientation and type of fracturing that generated the event. As a result, source mechanism inversions provide a much higher resolution set of parameters for building reservoir-scale discrete fracture network (DFN) models than can be derived from seismic attributes. DFN models are well established as tools to generate fracture flow properties

for reservoir simulation [1, 2] Fracture models used for reservoir characterization are often constructed by inferring a bulk fracture intensity based on seismic attributes such as seismic coherency or anisotropy, and a general orientation of fractures for relatively large volume elements can be defined using seismic velocity anisotropy [3, 4]. DFN models are also constrained by fracture data from wells, but this only provides information about the fracture character in a small portion of the reservoir [5, 6], and workers have developed various methods to extrapolate wellbore data to the reservoir scale [7, 8]. The use of well data and seismic attributes in the same reservoir model requires some method to upscale the well data to the bulk property scale data derived from the seismic attributes. Often the well scale is so small relative to the reservoir volume element that the correlation between fracture frequency measured along a well bore and a fracture intensity property derived from seismic data is extremely coarse and the resolution is insufficient for the type of well spacing decisions needed for development of unconventional reservoirs.

2. BACKGROUND

This study shows how microseismic events can provide direct measurement of the fracture orientation and how this orientation can be used to constrain DFN models. Microseismic event locations and source mechanisms provide direct information regarding fault plane failure (pure shear mechanism) or tensile opening (non-shear source mechanism). Thus, with source mechanisms of individual events, fractures can be created deterministically at the location of events and the fracture intensity in a volume can be directly related to the number of seismic events observed. This microseismically-constrained approach to fracture modeling takes advantage of data in an intermediate resolution range between that of seismic attributes and wellbore data. Utilizing both the locations of events and their source mechanisms to constrain DFN models facilitates high resolution simulation modeling that optimize field development and exploitation.

Hydraulic fracture treatments are often designed with the goal of creating tensile fractures from the wellbore, but the analysis of the patterns of microseismicity relative to the in situ stress field frequently shows the influence of pre-existing fractures. These pre-existing fractures can be reactivated in shear failure mode, and shear source mechanisms are typically reported from microseismicity generated by hydraulic fracturing [9, 10]. Tensile opening or closing events have been observed to occur during stimulation treatments, but these types of events are less frequently observed [11]. Despite the fact that tensile fracturing events are rarely identified by source mechanism inversions on microseismic data, the volume of incompressible proppant that is placed into the reserovoir indicates that they must occur. In one of the case studies presented in this paper, tensile fracturing is interpreted to occur and cause associated shear fracturing as the source of microseismic events. In the same example, source mechanisms indicating both dip slip on steeply dipping planes and reverse slip on shallowly dipping planes are identified, indicating that newly created tensile fracturing and reactivation of existing fractures are both sources of microseismicity. In a second case study, the method of "connecting the dots" of a trend of events and interpreting that trend to define a fracture plane fails upon examination of the source mechanisms from the events. The orientations and modes of failure indicated by the source mechanisms are different from the trends along which the events line up. Both case studies illustrate the importance of considering the geological context and deformational fabric of the rock, and how source mechanism inversions provide an import constraint for building fractured reservoir models.

3. CASE STUDY 1

The occurrence of different source mechanisms in the microseismicity induced during the treatment of a well drilled in the continental USA allowed us to identify different modes of fracturing and understand the stress current stress state in the reservoir. This stimulation was performed on a well at an approximate depth of 6000 ft and with approximately 4000 ft of horizontal section. The microseismic monitoring was carried out with the FracStar® surface array consisting of 9 lines 4000-7000 ft long. The surface monitoring array consisted of 980 single component receiver stations laid out with approximate 1:1 offset to depth ratio in a star-like pattern. Figure 1 shows a map view and vertical cross-section of the located microseismic events induced in all fracturing stages. While this dataset showed good signal-to noise quality, the resulting locations are difficult to interpret as fracture trends. The reverse mechanisms (orange spheres in Figure 1) show what appears to be upward growth of fracturing, with many of the events occurring above the wellbore. The dip-slip events (blue spheres in Figure 1) occur largely at the level of the wellbore.

The seismic response of the FracStar® shows some geophone locations detecting opposite polarity of the first ground motion of some of the large microseismic events. The analysis of the waveforms is done using the vertical component of the particle velocity. By picking the amplitudes and polarities of the first arrivals, maps were generated that show the relative amplitudes and polarity of the P-wave signal for two representative

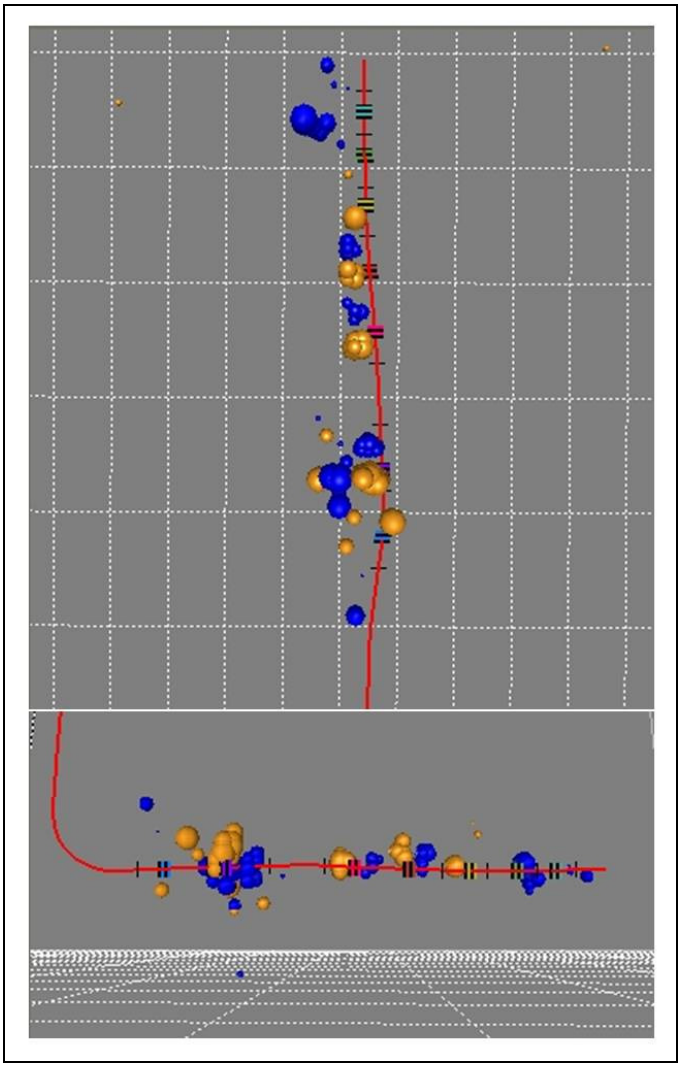

Figure 1. Map view (top) and vertical cross section (bottom) showing mapped locations of microseismic events. Events are colored by mechanism type, blue = dip slip on steeply dipping plane, orange = reverse slip on planes dipping 40-50°. Sphere size is proportional to event magnitude.

events (Fig. 2). Green symbols on the maps represent upward first motion, red symbols represent downward motion, and the relative amplitudes of the direct P-waves are represented by the circle size. Receivers without a reliable P-wave pick are not shown in these plots. Note that both size and polarity of the direct arrivals are smoothly varying with distance indicating both consistency of the picks as well as good consistent coupling of the geophones recording these waveforms.

The mechanism in the top plot in Figure 2 represents dip-slip along a nearly vertical fault plane striking 80° NE, with the northern side of the fault moving down. Other source mechanisms inverted for this case study have downward motion on the southern side of the fault. Strikes range from 80° to 70° degrees. The plot on the bottom of Figure 2 represents a reverse faulting mechanism. The failure plane for this and other mechanisms of this same type found in this example dip 45° to 50° degrees, and all have strike around 70° NE. On both plots the location of the event epicenter is shown by a small "beach-ball" (graphical representation of the P-wave radiation pattern of the event in a lower hemisphere stereographic projection), with a larger detail of that beach ball in the upper right corner of the plot.

The source mechanism inversion of these events used all picked arrivals fitted with modeled amplitudes in a homogeneous isotropic model with a free surface boundary condition. The two source mechanisms shown in Figure 2 represent pure-shear components of the general source mechanisms, that is, the double-couple component of the inverted full moment tensor. For each event of Figure 2 the pure shear components of the general mechanisms account for more than 90% of the released moment. Note that the inverted shear mechanism has a non-unique solution, resulting in two possible planes for the pure shear mechanism since slip motion along the two possible planes explains the observed data equally well.

The surface monitoring (i.e. the large number of the receivers in multiple offsets and azimuths) allowed us to study in detail the shear and non-shear ratio in the source mechanisms. The wide aperture sampling of the focal sphere possible with the surface monitoring technique has detected events where non-shear mechanisms provide significantly better fit to the observed data, but no events of this type were detected in this case study.

Table 1. Summary of shear planes and rakes from inverted source mechanisms

Source Mechanism	Dips	Strikes	Rakes
Dip Slip North Side Up	88 10	65 165	-80 -170
Dip Slip North Side Down	88 5	85 195	95 20
Reverse Slip Northeast Strike	41 50	50 245	78 100
Reverse Slip Northeast Strike	45 47	95 254	105 75

Table 1 summarizes information about the orientation of the shear planes and rakes of the inverted mechanisms. The inversion provides remarkably stable dips (less than 2° difference for inverted dips), strikes, and rakes (less than 10° difference for the steeply dipping planes). If we assume that the steeply dipping dip slip shear events are occurring on nearly vertical but not exactly vertical planes, then the mechanism with the north side up is interpreted to be normal while the mechanism with the north side down is reverse. It is not possible to explain the existence of both failure mechanisms within the same stress field. However, dips of both of these mechanisms are very close to vertical so that within the

inversion uncertainty (which also includes location) they could be interpreted to be either vertical or dipping a few degrees in the opposite direction. Deviations of the rakes from 90° (which represents pure dip-slip) would indicate a significant non-vertical orientation of the one of the principle stresses. All of the source mechanisms show that one of the principal stresses is close to vertical (Table 1). If the shear planes are not vertical and have opposing dip directions they could represent conjugate fracturing of opposite motion on the fault planes. This type of relationship has been observed for microseismicity in The Cotton Valley Limestone [9] and was attributed to right-lateral strike-slip motion along fractures associated with the hydraulically-opened tensile fractures that have failure planes closely aligned with, but not parallel to, the fracture trend.

The seemingly contradictory dip slip source mechanisms in this dataset may also involve reactivation of existing natural fractures. The best candidate for the activated natural (pre-existing) fault plane is the moderately dipping reverse faulting source mechanisms. Because it is not possible for normal dip slip and reverse faulting to occur in the same stress field, we assume that the unequivocal reverse failure mechanisms indicate the tectonic stress: vertical stress is the minimum stress. This constrains the mechanisms on the steeply dipping planes to be reverse displacement as well, thereby allowing us to interpret beyond the uncertainty in the source mechanism solution. We interpret the steeply dipping failure planes to be caused by slip associated with tensile opening of fractures parallel to bedding.

Horizontal fracturing may take advantage of pre-existing planes of weakness in the rock, as oil and gas shales often have a very strong horizontal fabric that can be enhanced by the formation of hydrocarbons [12]. The upward displacement of bedding layers results in the formation of a mini-popup above the horizontal fracture (Figure 3), facilitated by existing natural fractures that are essentially perpendicular to bedding. The magnitude of the seismic response of tensile failure is too small to be detected in this study, but the source mechanism comes from the associated shear fracturing.

The strike of the shear planes from the reverse slip source mechanisms also allow us to infer the orientation of the maximum horizontal stress to be NW-SE (Fig. 3, bottom). Because of the range of strikes observed for the different source mechanisms, it is likely that most of the failure planes on both types of source mechanisms are taking advantage of existing fracture planes in the rock.

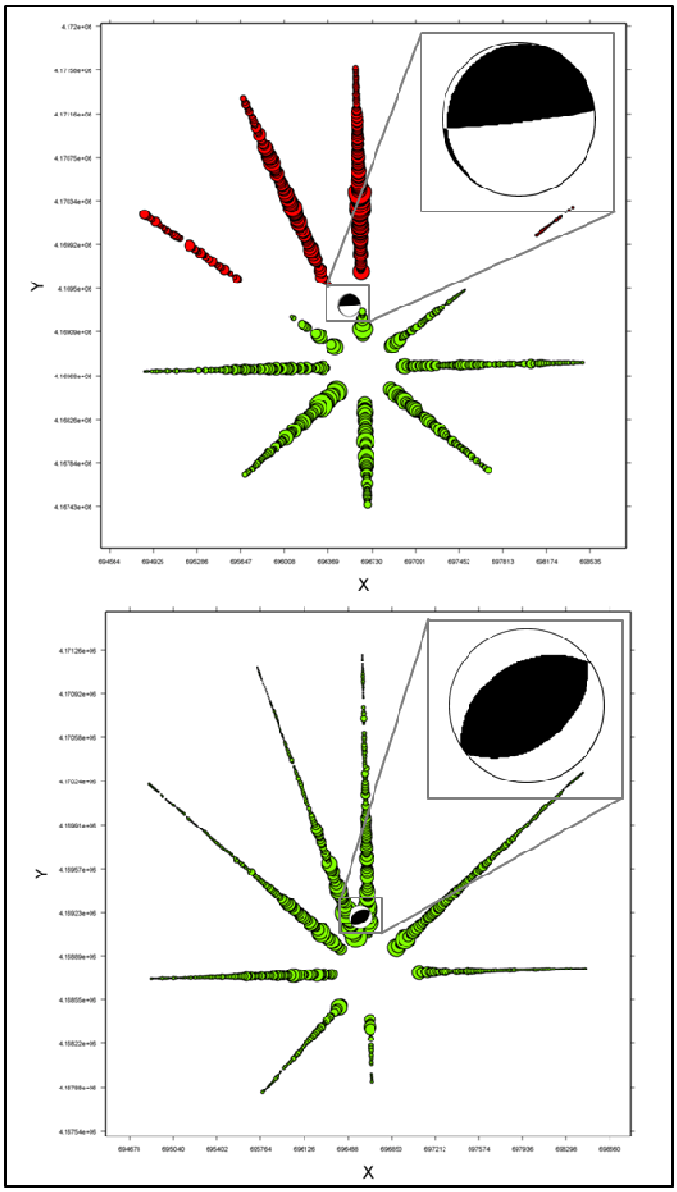

Figure 2. Map views of the polarity response of the seismic acquistion array showing the relative sizes of the first arrivals for two types of induced microseismic events. Red circles represent motion down; green circles motion up. Circles size is proportional to the observed relative amplitudes. Beach balls in upper right of each plot are enlarged to show the details of the source mechanisms, with the epicenter location show by the small beach balls plotted near the center of the array.

3.1. DFN Model Using Source Mechanisms

In addition to the conceptual validation that is possible by visualizing a 3 dimensional discrete fracture network (DFN) represented by the microseismicity, modeling the flow behavior of the stimulated reservoir can be facilitated with such models. Properties such as fracture permeability, fracture porosity and fracture connectivity can be calculated from the DFN and used to

populate

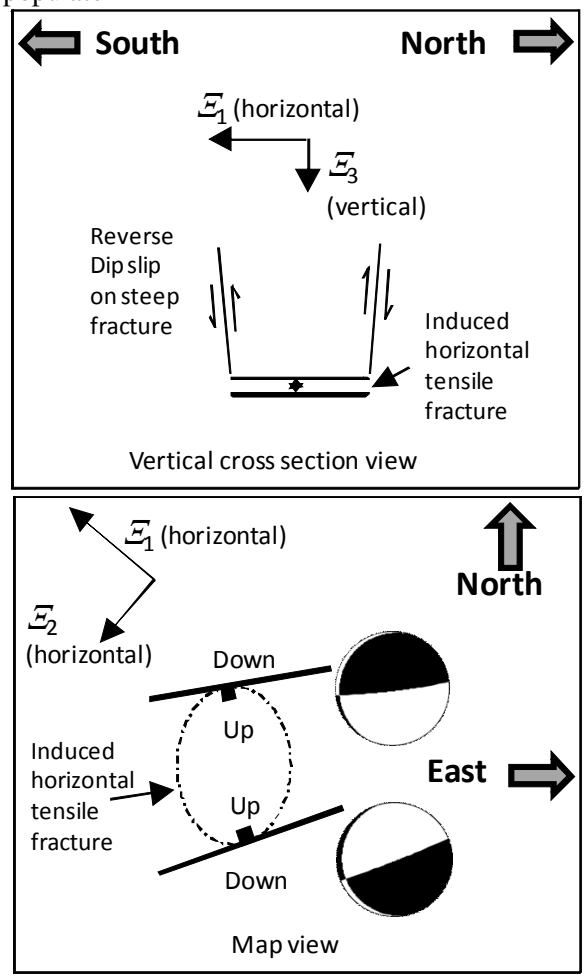

Figure 3. Schematic drawing of failure mechanisms related to horizontal fracturing during hydraulic stimulation. Minimum stress is vertical. NW oriented maximum compressive stress is approximate and is inferred from strike of the reverse slip source mechanisms.

reservoir simulation grids. Figure 4 shows a fracture network constrained by the event locations and mechanisms discussed above. In general, fracture size is poorly constrained by wellbore and reflection seismic data attributes, but by using the seismic moment of the events, a reasonable estimate of fracture size per event can be made. The largest fractures in Figure 5 have dimensions in the range of 10^1 meters, based on rupture sizes associated with small magnitude events (< magnitude 1) from observations of small induced reservoir earthquakes[13, 14].

The green fractures in Figure 4 represent the moderately dipping reverse slip shear planes, and the relative length of the fracture sizes show the higher energy associated with these shear events. The blue fracture planes represent the steeply dipping dip slip failure plane that we interpret to be activated by the horizontal tensile fractures represented in red. Horizontal fractures of this type could create a significant contribution to flow in a

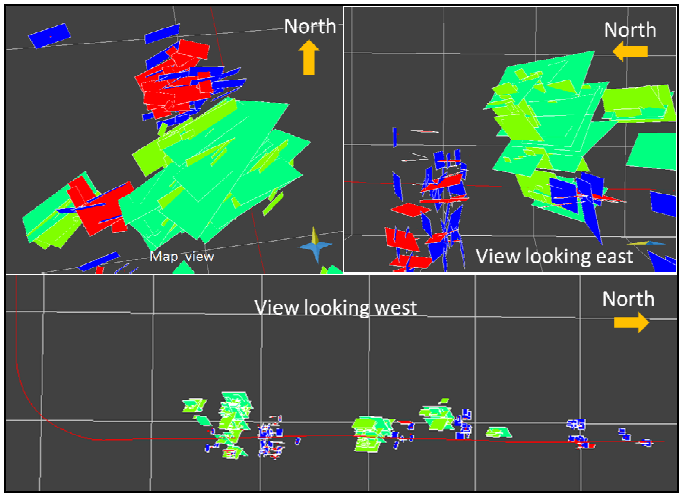

Figure 4. Discrete fracture network generated from microseismic event locations and inverted source mechanisms. Top left picture is a map view. Green and turquoise fractures on the reverse slip mechanism planes. Right top picture shows vertical view looking toward the east, showing detail of horizontal fracture planes and steeply dipping dip slip planes. The bottom picture shows DFN for all stages of the fracture treatment displayed along the wellbore lateral; view is toward the west.

reservoir that may impact the success of the history matching exercise. This process-based fracture constraint allows us to identify the possibility of these fractures and include them in the DFN.

4. CASE STUDY 2

In a vertical well in the mid-continent USA with well defined trends developed in the patterns of microseismicity, we were able to indentify complex fracturing behavior during a hydraulic fracturing stimulation. Near the beginning of pumping during the frac treatment distinct E-W trend develops in the microseismicity away from the well and some time into the treatment, a second trend oriented SE-NW develops. Microseismic activity continues to occur along both trends through the end of the treatment, so the final result has two well developed trends of events extending on either side of the well, but with approximately 30^o difference in orientation (Figure 5). The vertical spread of the events suggests that the microseismicity occurs along fault or fracture planes. A crossed-dipole sonic log analysis revealed two directions of fast shear wave polarization, a nearly E-W direction interpreted to be parallel to natural fractures intersecting the borehole, and a SE-NW direction interpreted to be parallel to the maximum horizontal stress direction. A Stonely wave log was acquired in this borehole which also indicated the presence of open fractures in the reservoir.

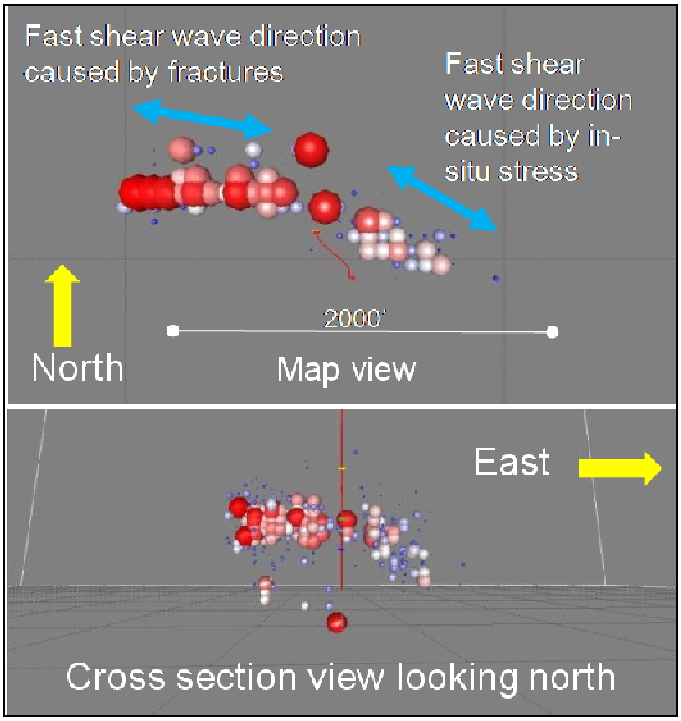

Figure 5. Trends of microseismicity for a one-stage fracture stimulation treatment, showing a change in direction near the wellbore location (top picture). Anisotropy measured in the borehole with crossed dipole sonic log show two different fast shear wave directions, one attributed to natural fractures in the rock and the other to the maximum horizontal stress direction. Bottom picture is a cross section view showing the vertical distribution of events.

If the microseismicity trends have developed along pre-existing fault planes, the simple interpretation is two steeply dipping and intersecting fault planes. Their geometry is consistent with the E-W fault being reactivated in strike-slip displacement with slip on the E-W fault migrating along the fault plane until it intersected the SE striking normal fault (Fig. 6). This type of fault interaction is commonly observed in structural geology analysis as a "releasing bend". The timing of the microseismicity during the treatment showing the activity first commencing on the E-W trend of events before the SE trend develops is also consistent with this interpretation.

In order to verify this simple geologic interpretation, a source mechanism inversion was done on the representative event in each orientation trend. The largest events were visible in the raw seismic data, and a change in polarity along three of the arms of the array can be seen (Fig. 7, top). The azimuth of the failure plane can be seen in the map of the surface array response plotted with red indicating first motion up and blue first motion down (Fig. 7, bottom). Because this array is centered about a vertical well, and a large distance is spanned by the array on the surface, all of the epicenter locations are in the middle of the array. The location of the line of polarity change, however is

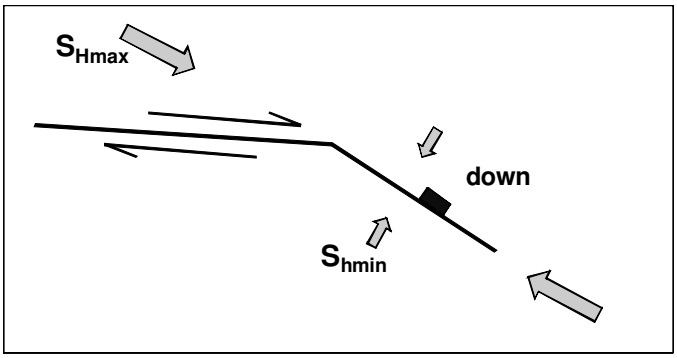

Figure 6. Simple geologic explanation for trends in microseismicity developed during treatment of the vertical well in case study 2. The interaction between the strike-slip fault and the normal fault is a classic structural geology example of a releasing bend fault interaction.

roughly 1000 feet to the south of the epicenters, indicating a moderately dipping failure plane.

The source mechanism inversions confirmed that shear planes striking approximately E-W are active in this data, but they have moderate dips of 40° or 50° and the sense of shear is dip slip, not strike-slip so it does not fit the releasing bend model (Fig. 8). Even more complexity is shown by the source mechanism inversion of the event from the SE trending microseismicity. The strike of the shear plane for this event is not parallel to the trend of events, but rather it also approximately E-W. These planes also have moderate dips, either 30° or 60°. Because both source mechanisms are dip slip normal faulting, the maximum stress is vertical.

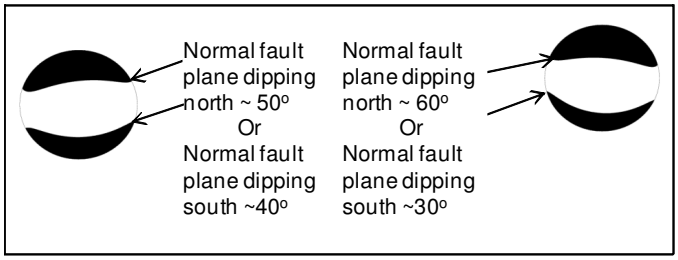

Figure 7. Two source mechanisms from case study 2 showing both failure mechanisms are normal dip slip shear. The beach ball on the left is for the largest event in the E-W trend of microseismicity, the right beach ball is for the largest event from the SE trend of microseismicity.

It is possible that the two largest events were from fractures that were oriented differently from the rest of the microseismicity-generating fractures in each trend. To test this possibility, we ran a matched filter processing on the data to test whether the source mechanisms on either side of the bend in the trend of events were not typical. The matched filter processing showed that all of the events have the same type of source mechanism, dip slip on planes that strike roughly E-W. Figure 9 shows a possible DFN configuration

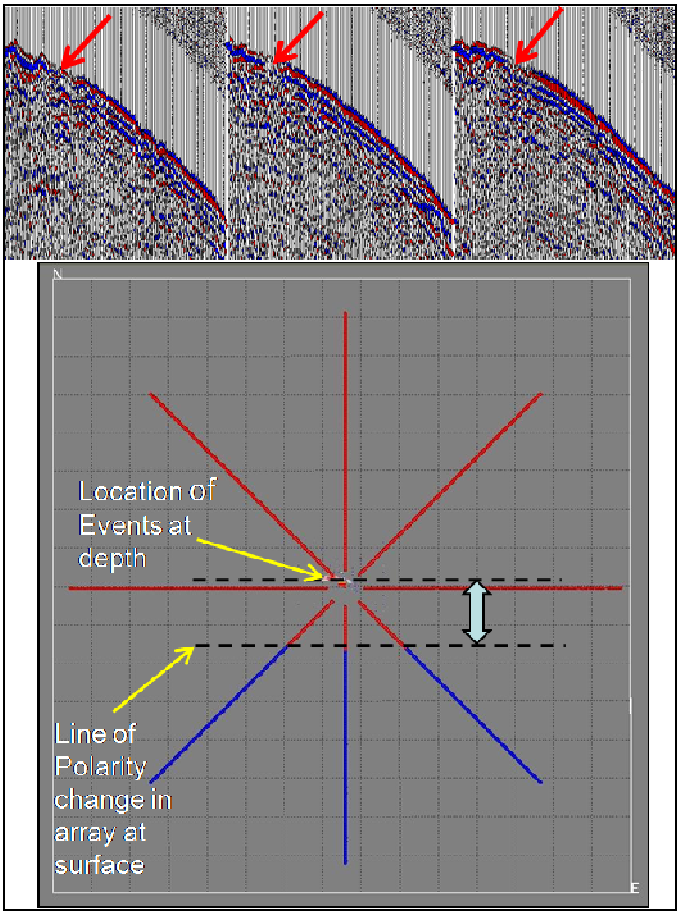

Figure 8. Seismic lines from the three arms of the array with a change in polarity, indicated by the red arrows (top). Map of surface array (bottom) showing location of polarity change on the three arms. Event epicenters are near the center of the array, approximately 1000' north of the polarity change, indicating a dipping shear failure plane.

based on the event locations and the two source mechanisms with slightly different strikes for the two different trends of events. The complexity of the fracturing of shows that fitting a plane to the microseismicity event trends results in a fracture model that is too simple. The trends of events are composed of en-echelon interacting small fractures that are oriented at an angle to the overall event trend. The moderately dipping source mechanisms are interpreted to be shear failure on existing natural fractures reactivated by the stimulation treatment. The spatial distribution of the fracture network is interpreted to be constrained by the existence of two faults in the orientations shown in the simple geologic interpretation (Fig. 6). The fractures that are activated in the treatment, however, are the likely damage zone small fractures that form around faults.

When the distribution of all magnitudes in the microseismic data is analyzed for their frequency of occurrence, they can be seen to follow a power law distribution (Fig. 10, left). This kind of size versus frequency of occurrence is observed for naturally-occurring earthquakes [15]. Natural fracture populations also have a power law distribution of lengths [16, 17]. Because we interpret the microseismicity to emanate from reactivation of existing natural fractures, the fractures comprising the DFN were modeled with a power-law distribution (Fig. 10, right).

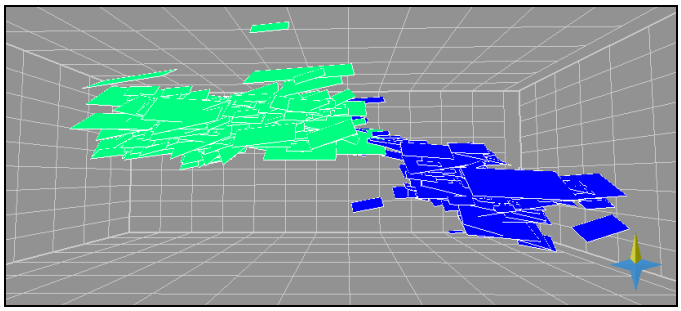

Figure 9. DFN realization of possible fracture network based on microseismic event locations and source mechanisms. Strike of E-W trend (green fractures) is WSW, strike of SE trend is ESE.

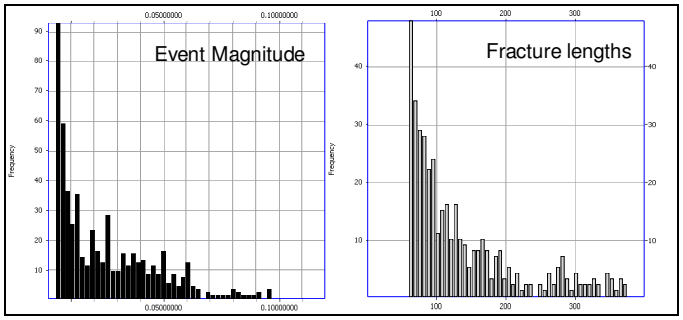

Figure 10. Frequency histogram of event moment and fracture lengths for fractures constrained by microseismic events.

5. CONCLUSIONS

Source mechanism characterizations in the first case study presented in this paper allowed us to determine the stress state of the reservoir. In particular, the determination was made in the absence of borehole stress measurements in a tectonically active region where the regional stress shows a wide variability of orientations. The local in-situ stress is important for understanding the induced fracture behavior and evaluating its extent and effectiveness. An unexpected result was the strong evidence for horizontal tensile fracturing, which is contrary to the assumption of a vertical maximum stress that is reasonable for many sedimentary basins.

The second case study shows an example where the microseismic interpretation based on the geometry of the locations leads to a serious underestimate of the volume of stimulated reservoir. The source mechanism inversions indicate that the induced microseismicity comes not from fractures that are parallel to the trends of microseismicity, but from shear planes that are at an angle to the trend. Moderately dipping shear failure planes also indicate that the microseismicity is not generated by newly created tensile fractures, but rather

from reactivation of and interaction with existing fractures in the roc. The simple "connect the dots" approach to interpreting the fracture as a single large failure plane breaks down in when the source mechanism inversions show significantly different fracture orientations. The added complexity of the discrete fracture geometry is a positive outcome for reservoir stimulation, as the treatments are more effective if they are able to plug into the existing plumbing of the rock.

These studies represent cases where the failure mechanisms that occurred in the hydraulic fracturing treatment indicate very different fracture orientations than those that might be interpreted from the trends of events. In both cases, the impact of the existing natural fractures strongly influence the type of fracturing observed in the rock. By integrating geological factors with the geometric requirements of the failure mechanisms, we were able to reduce the uncertainty related to the source mechanism inversions and determine the most likely orientation and failure modes of fractures in the reservoir. By combining the source mechanisms inversions with the geological solution we were able to derive a fracturing model that is consistent with the stress data from the reservoir and with the source mechanisms.

The authors would like to thank Jo Ellen Kilpatrick, BJ Hulsey, and Andrew Hill for their help and careful processing and analysis of the microseismic data.

REFERENCES

1. Dershowitz, B., LaPointe, P., Eiben, T., Wei, L., 1998, Integration of discrete feature network methods with conventional simulator approaches, SPE-49069-MS
2. Karimi-Fard, M., Durlofsky, L.J., Aziz, K., 2004, An efficient discrete-fracture model application for general-purpose reservoir simulators, SPE-88812-PA
3. Wong, P., 2003, A novel technique for modeling fracture intensity: A case study from the Pinedale anticline in Wyoming, AAPG Bulletin, e. 87, no. 11, pp. 1717-1727.
4. Jenkins, C., Ouenes, A., Zellou, A., and Wingard, J., 2009, Quantifying and predicting naturally fractured reservoir behavior with continuous fracture models, AAPG Bulletin, v. 93, no. 11, pp. 1597-1608.
5. Prioul R. and Jocker J., 2009, Fracture characterization at multiple scales using borehole images, sonic logs, and walkaround vertical seismic profile: AAPG Bulletin, **93**, no. 11, pp. 1503–1516.
6. Wu, H., and Pollard, D. D., 2002, Imaging 3-D fracture networks around boreholes, AAPG Bulletin, v. 86, no. 4, pp. 593-604.
7. Narr, W., 1996, Estimating average fracture spacing in subsurface rock, AAPG Bulletin, v. 80, no. 10, p. 1565-1586
8. Ortega, O. J., Marrett, R. A., and Laubach, S. E., 2006, A scale-independent approach to fracture intensity and average spacing measurement, AAPG Bulletin, v. 90, no. 2, pp. 193-208.
9. Rutledge, J. T., and W.S. Phillips, W. S., (2003), Hydraulic stimulation of natural fractures as revealed by induced microearthquakes, Carthage Cotton Valley gas field, east Texas, : Geophysics, 68, 441 – 452, doi: 10.1190/1.1567212.
10. Pearson, C., 1981, The relationship between microseismicity and high pore pressures during hydraulic stimulations experiments in low permeability granitic rocks, : J. Geophys. Res., 86, 7855 – 7864, doi: 10.1029/JB086iB09p07855.
11. Julian, B. R., G. R. Foulger, and F. Monastero (2007), Microearthquake moment tensors from the Coso Geothermal area, in Proceedings, Thirty-Second Workshop on Geothermal Reservoir Engineering, Paper SGP-TR-183, Stanford Univ., Stanford, Calif.
12. Lash, G. G., and Engelder, T. 2005, An analysis of horizontal microcracking during catagenesis: Example from the Catskill delta complex, AAPG Bulletin, v. 89, no. 11, pp. 1433-1449
13. Tomic, J., Abercrombie, R. E., and Nascimento, A. F., 2009, Source parameters and rupture velocity of small M≤=2.1 reservoir induced earthquakes, Geophysics Journal International, …
14. Aki, K., and Richards, P. G., 2002, *Quantitative Seismology*, University Science Books, Sausalito, CA.
15. Lay, T. and Wallace, T.C., 1995, Earthquake Statistics. In *Modern Global Seismology,* Academic Press, San Diego, CA.
16. Sweetkind, D.S., Anna, L.O., Williams-Stroud, S.C., and Coe, J.A., Characterizing the fracture network at Yucca Mountain, Nevada. Part 1. Integration of field data for numerical simulations, RMAG 1997 Guidebook, ed. T. E. Hoak, A. L. Klawitter, and P. K. Blomquist, pp. 185- 196.
17. Vermilye, J. M., and Scholz, C. H., 1995, Relation between vein length and aperture, Journal of Structural Geology, v. 17, no. 3, pp. 423-434.